ASME2015 IDETC/CIE, 11th International Conference on Multibody Systems, Nonlinear Dynamics, and Control (MSNDC)

MSNDC-10 Vehicle Dynamics

Technical Publication

DEVELOPMENT OF SHEAR DEFORMABLE LAMINATED SHELL ELEMENT AND ITS APPLICATION TO ANCF TIRE MODEL

Hiroki Yamashita
Department of Mechanical and Industrial Engineering
The University of Iowa
2312 Seamans Center
Iowa City, IA 52242

Paramsothy Jayakumar
US Army TARDEC
6501 E. 11 Mile Road
Warren, MI 48397-5000

Hiroyuki Sugiyama
Department of Mechanical and Industrial Engineering
The University of Iowa
2416C Seamans Center
Iowa City, IA 52242
hiroyuki-sugiyama@uiowa.edu

Report Documentation Page

Form Approved
OMB No. 0704-0188

1. REPORT DATE	2. REPORT TYPE	3. DATES COVERED
24 APR 2015		**00-00-2015 to 00-00-2015**

4. TITLE AND SUBTITLE	5a. CONTRACT NUMBER
Development of Shear Deformable Laminated Shell Element and its Application to ANCF Tire Model	5b. GRANT NUMBER
	5c. PROGRAM ELEMENT NUMBER
6. AUTHOR(S)	5d. PROJECT NUMBER
	5e. TASK NUMBER
	5f. WORK UNIT NUMBER
7. PERFORMING ORGANIZATION NAME(S) AND ADDRESS(ES) **US Army RDECOM-TARDEC,6501 E. 11 Mile Road,Warren,MI,48397-5000**	8. PERFORMING ORGANIZATION REPORT NUMBER
9. SPONSORING/MONITORING AGENCY NAME(S) AND ADDRESS(ES)	10. SPONSOR/MONITOR'S ACRONYM(S)
	11. SPONSOR/MONITOR'S REPORT NUMBER(S)

12. DISTRIBUTION/AVAILABILITY STATEMENT
Approved for public release; distribution unlimited

13. SUPPLEMENTARY NOTES
ASME 2015 IDETC/CIE, 11th International Conference on Multibody Systems, Nonlinear Dynamics, and Control (MSNDC)

14. ABSTRACT
See Report

15. SUBJECT TERMS

16. SECURITY CLASSIFICATION OF:			17. LIMITATION OF ABSTRACT	18. NUMBER OF PAGES	19a. NAME OF RESPONSIBLE PERSON
a. REPORT	b. ABSTRACT	c. THIS PAGE			
unclassified	**unclassified**	**unclassified**	**Same as Report (SAR)**	**29**	

ABSTRACT

In this investigation, a continuum mechanics based shear deformable shell element of the absolute nodal coordinate formulation (ANCF) is generalized to a laminated shell element for application to the modeling of fiber-reinforced rubber (FRR) structure of the physics-based ANCF tire model. The complex deformation coupling exhibited in fiber-reinforced composite materials can be automatically considered in the shear deformable laminated shell element using the continuum mechanics approach, and the element lockings are systematically eliminated by the assumed natural strain and enhanced strain approaches, thereby leading to a locking-free shear deformation ANCF laminated shell element. Furthermore, various nonlinear material models can be considered for each layer in a way same as solid elements. Using the ANCF laminated shell element developed, a physics-based ANCF tire model is developed by considering the detailed tire geometry and material properties. The experimental validation of the tire model is conducted for the load-deflection curve to ensure that the fundamental structural tire properties can be correctly captured in the ANCF tire model.

1. INTRODUCTION

An accurate modeling of the complex tire geometry and the anisotropic material properties of tires is essential to the tire performance evaluation including the tire contact pressure and the braking/traction and cornering forces. Since a tire consists of layers of plies and steel belts embedded in rubber, the tire structure needs to be modeled by cord-rubber composite materials and various fiber-reinforced rubber material models are proposed for use in detailed finite element tire models. Since Young's modulus of the steel cord is significantly higher than that of the rubber matrix, mechanical property of the fiber-reinforced rubber (FRR) is highly nonlinear [1]. In particular, the tire cross-section property that includes the geometric and material properties is of significant importance in characterizing the normal contact pressure distribution. Furthermore, the in-plane shear deformation of the carcass contributes to the cornering characteristics of tires. For this reason, large-dimensional high-fidelity finite element tire models that account for the tire geometric and material nonlinearities are developed and used for the tire performance evaluation. However, existing finite element tire models cannot be integrated into the vehicle dynamics simulation due to the essential difference in formulations and solution procedures used in multibody dynamics and nonlinear finite element codes. This prevents an integration of the high-fidelity tire model into the multibody vehicle dynamics simulation [2] and, therefore, the structural characteristics of tires and transient tire dynamics are, in general, evaluated using different computational models and different simulation approaches. To overcome this fundamental and essential problem in the tire dynamics simulation, a tire model based on the flexible multibody dynamics approach [2-4] is developed using the absolute nodal coordinate formulation (ANCF [6, 7]). The in-plane ANCF-LuGre tire model developed for the transient braking analysis allows for considering the nonlinear coupling between the dynamic

structural deformation of the tire and its transient tire force in the contact patch using general multibody dynamics computer algorithms [4]. The generalization of the in-plane ANCF tire model to the three-dimensional model requires the development of the new ANCF shell element suited for the tire model, which allows for modeling the nonlinear fiber-reinforced rubber materials and the accurate three-dimensional stresses under various maneuvering scenarios. To this end, the continuum mechanics based shear deformable shell element of the absolute nodal coordinate formulation (ANCF) [5] is generalized to a laminated shell element in this study for application to the modeling of fiber-reinforced rubber (FRR) structure of the physics-based ANCF tire model. Furthermore, a physics-based ANCF tire model is developed using the shear deformable laminated shell elements such that the high-fidelity tire model can be integrated into general multibody dynamics computer algorithms for ground mobility simulation.

2. CONTINUUM MECHANICS BASED SHEAR DEFORMABLE ANCF SHELL ELEMENT

2.1 Kinematics of ANCF Shell Element

As shown in Fig. 1, the global position vector $\mathbf{r}^i$ of a material point $\mathbf{x}^i = [x^i \quad y^i \quad z^i]^{\mathrm{T}}$ in shell element *i* is defined as [5]

$$\mathbf{r}^i = \mathbf{r}_m^i(x^i, y^i) + z^i \frac{\partial \mathbf{r}^i}{\partial z^i}(x^i, y^i) \tag{1}$$

where $\mathbf{r}_m^i(x^i, y^i)$ is the global position vector in the middle surface and $\partial \mathbf{r}^i(x^i, y^i)/\partial z^i$ is the transverse gradient vector used to describe the orientation and deformation of the infinitesimal volume in the element. Using the bi-linear polynomials, the position vector in the middle surface and the transverse gradient vector are approximated as follows:

$$\mathbf{r}_m^i(x^i, y^i) = \mathbf{S}_m^i(x^i, y^i)\mathbf{e}_p^i, \qquad \frac{\partial \mathbf{r}^i}{\partial z^i}(x^i, y^i) = \mathbf{S}_m^i(x^i, y^i)\mathbf{e}_g^i \tag{2}$$

where $\mathbf{S}_m^i = \begin{bmatrix} S_1^i\mathbf{I} & S_2^i\mathbf{I} & S_3^i\mathbf{I} & S_4^i\mathbf{I} \end{bmatrix}$ and

$$S_1^i = \frac{1}{4}\left(1-\xi^i\right)\left(1-\eta^i\right),\ S_2^i = \frac{1}{4}\left(1+\xi^i\right)\left(1-\eta^i\right),\ S_3^i = \frac{1}{4}\left(1+\xi^i\right)\left(1+\eta^i\right),\ S_4^i = \frac{1}{4}\left(1-\xi^i\right)\left(1+\eta^i\right) \tag{3}$$

where $\xi^i = 2x^i / \ell^i$ and $\eta^i = 2y^i / w^i$. ℓ^i and w^i are lengths along the element x^i and y^i axes, respectively. In Eq. 2, the vectors $\mathbf{e}_p^i$ and $\mathbf{e}_g^i$ represent the element nodal coordinates associated with the global position vector in the middle surface and the transverse gradient vector. That is, for node *k* of element *i*, one has $\mathbf{e}_p^{ik} = \mathbf{r}^{ik}$ and $\mathbf{e}_g^{ik} = \partial \mathbf{r}^{ik} / \partial z^i$.

In the continuum mechanics approach, the elastic forces of the shell element are evaluated as a continuum volume and the Green-Lagrange strain tensor **E** at an arbitrary material point in element *i* is defined as follows:

$$\mathbf{E}^i = \frac{1}{2}\left((\mathbf{F}^i)^T\mathbf{F}^i - \mathbf{I}\right) \tag{4}$$

where $\mathbf{F}^i$ is the global position vector gradient tensor. The preceding equation can be expressed in terms of the covariant strain tensor $\tilde{\mathbf{E}}^i$ as

$$\mathbf{E}^i = (\mathbf{J}^i)^{-T}\tilde{\mathbf{E}}^i(\mathbf{J}^i)^{-1} \tag{5}$$

where $\mathbf{J}^i = \partial \mathbf{X}^i / \partial \mathbf{x}^i$ and $\mathbf{X}^i$ represents the global position vector of element *i* at an arbitrary reference configuration. The covariant strain tensor is defined as

$$\tilde{\mathbf{E}}^i = \frac{1}{2}\left((\bar{\mathbf{J}}^i)^T\bar{\mathbf{J}}^i - (\mathbf{J}^i)^T\mathbf{J}^i\right) \tag{6}$$

where $\bar{\mathbf{J}}^i = \partial \mathbf{r}^i / \partial \mathbf{x}^i$. Using Eq. 5, the strain vector $\boldsymbol{\varepsilon}^i = [\varepsilon_{xx}^i \quad \varepsilon_{yy}^i \quad \gamma_{xy}^i \quad \varepsilon_{zz}^i \quad \gamma_{xz}^i \quad \gamma_{yz}^i]^T$ is defined as

$$\boldsymbol{\varepsilon}^i = (\mathbf{T}^i)^{-T} \tilde{\boldsymbol{\varepsilon}}^i \tag{7}$$

where $\tilde{\boldsymbol{\varepsilon}}^i$ is the covariant strain vector obtained by Eq. 6, and the transformation matrix $\mathbf{T}^i$ is as given in literature [5].

2.2 Generalized Elastic Forces

In the continuum mechanics based shear deformable ANCF shell element, element lockings occur due to the use of low-order polynomials, resulting in erroneously stiffer bending behavior. The locking in the continuum mechanics based shear deformable ANCF shell element includes the transverse shear locking; Poisson's thickness locking; curvature thickness locking; in-plane shear locking [5]. These lockings are systematically alleviated by applying the assumed natural strain [8, 9] and the enhanced assumed strain approaches [10, 11]. The modified strain field for the continuum mechanics-based shear deformable ANCF shell element can then be defined as follows [5]:

$$\hat{\boldsymbol{\varepsilon}} = \mathbf{T}^{-T} \tilde{\boldsymbol{\varepsilon}} + \boldsymbol{\varepsilon}^{EAS} \tag{8}$$

where the covariant transverse normal and shear strains are evaluated by the assumed strain approach, while the other covariant strains are evaluated as compatible strains obtained directly from the assumed global displacement field. This leads to the following covariant strain vector:

$$\tilde{\boldsymbol{\varepsilon}} = \begin{bmatrix} \tilde{\varepsilon}_{xx} & \tilde{\varepsilon}_{yy} & \tilde{\gamma}_{xy} & \tilde{\varepsilon}_{zz}^{ANS} & \tilde{\gamma}_{xz}^{ANS} & \tilde{\gamma}_{yz}^{ANS} \end{bmatrix}^T \tag{9}$$

The enhanced assumed strain vector $\boldsymbol{\varepsilon}^{EAS} = \begin{bmatrix} \varepsilon_{xx}^{EAS} & \varepsilon_{yy}^{EAS} & \gamma_{xy}^{EAS} & \varepsilon_{zz}^{EAS} & 0 & 0 \end{bmatrix}^T$ in Eq. 8 is defined as [10, 11]

$$\boldsymbol{\varepsilon}^{EAS} = \frac{|\mathbf{J}_0|}{|\mathbf{J}(\boldsymbol{\xi})|} \mathbf{T}_0^{-\mathrm{T}} \mathbf{N}(\boldsymbol{\xi}) \boldsymbol{\alpha} \tag{10}$$

where $\mathbf{J}(\boldsymbol{\xi})$ and $\mathbf{J}_0$ are the global position vector gradient matrices at the reference

configuration evaluated at the Gaussian integration point $\boldsymbol{\xi}$ and at the center of element ($\boldsymbol{\xi} = \mathbf{0}$), respectively. $\boldsymbol{\xi}$ is a vector of the element coordinates in the parametric domain and $\mathbf{T}_0$ is the constant transformation matrix evaluated at the center of element. The matrix $\mathbf{N}(\boldsymbol{\xi})$ defines polynomials for the enhancement of the strain field in the parametric domain and $\boldsymbol{\alpha}$ is a vector of internal parameters associated with the interpolating polynomials $\mathbf{N}(\boldsymbol{\xi})$ of the enhanced strain field. The generalized elastic forces of the shell element are obtained as a continuum solid using the virtual work as follows:

$$\mathbf{Q}_s^i = -\int_{V_0^i} \left(\frac{\partial \boldsymbol{\varepsilon}^i}{\partial \mathbf{e}^i} \right)^T \frac{\partial W^i(\hat{\boldsymbol{\varepsilon}}^i)}{\partial \boldsymbol{\varepsilon}^i} dV_0^i \tag{11}$$

where dV_0^i is the infinitesimal volume at the reference configuration of element *i*, and W is an elastic energy density function. The continuum mechanics based shear deformable ANCF shell element allows for considering general hyperelasticity material models in a way same as existing solid elements.

3. LAMINATED SHELL FORMULATION

3.1 Classical Lamination Theory

In fiber-reinforced composite materials that are widely used in many engineering applications, laminae having different fiber angles are bonded together to produce desired material properties. Since many laminae are stacked at different fiber angles, the complex deformation coupling between the extension, shearing, bending and twisting occurs, and such a deformation coupling characterizes the mechanical behavior of fiber-reinforced composite materials [12]. In the first part of this section, the macro-mechanical behavior of fiber-reinforced composite materials is overviewed using the classical lamination theory.

In the Kirchhoff plate theory, the plane stress is assumed and the in-plane strains of a plate $\boldsymbol{\varepsilon}_p = [\varepsilon_{xx} \quad \varepsilon_{yy} \quad \gamma_{xy}]^T$ are defined as

$$\boldsymbol{\varepsilon}_p = \boldsymbol{\varepsilon}_p^0 + z\boldsymbol{\kappa} \tag{12}$$

where $\boldsymbol{\varepsilon}_p^0 = [\varepsilon_{xx}^0 \quad \varepsilon_{yy}^0 \quad \gamma_{xy}^0]^T$ is a vector of the in-plane strains in the middle plane, and $\boldsymbol{\kappa} = [\kappa_x \quad \kappa_y \quad \kappa_{xy}]^T$ is a curvature vector associated with bending and twisting. Using a linear orthotropic constitutive law, the in-plane stress vector is related to its strain vector by $\boldsymbol{\sigma}_p = \mathbf{C}_p \boldsymbol{\varepsilon}_p$, and the material moduli is given as [12]

$$\mathbf{C}_p = \mathbf{R}^{-1} \bar{\mathbf{C}}_p \mathbf{R}^{-T} \tag{13}$$

In the preceding equation, the transformation matrix $\mathbf{R}$ is a function of the fiber angle θ that defines the orientation of the fiber coordinate system *o*-12 with respect to the material frame *o-xy* of the plate as shown in Fig. 1. This matrix is defined by

$$\mathbf{R} = \begin{bmatrix} \cos^2\theta & \sin^2\theta & \sin 2\theta \\ \sin^2\theta & \cos^2\theta & -\sin 2\theta \\ -\sin 2\theta & \sin 2\theta & \cos 2\theta \end{bmatrix} \tag{14}$$

and $\bar{\mathbf{C}}_p$ is the material moduli of an orthotropic material in the fiber coordinate system as

$$\bar{\mathbf{C}}_p = \begin{bmatrix} \bar{C}^{1111} & \bar{C}^{1122} & 0 \\ \bar{C}^{1122} & \bar{C}^{2222} & 0 \\ 0 & 0 & \bar{C}^{1212} \end{bmatrix} \tag{15}$$

where $\bar{C}^{1111} = E_1(1-\nu_{12}\nu_{21})$, $\bar{C}^{2222} = E_2(1-\nu_{12}\nu_{21})$, $\bar{C}^{1122} = \nu_{21}E_1(1-\nu_{12}\nu_{21})$, and $\bar{C}^{1212} = G_{12}$. While the coupling terms between the normal and shear strains in the fiber coordinate system are zero as observed in Eq. 15, the extension and shear coupling occurs for the stress and strain field defined in the material frame and the coupling terms in the material moduli matrix $\mathbf{C}_p$ of Eq. 13

are not zero. That is, a plate subjected to a uniaxial load produces in-plane shear deformation due to the extension and shear coupling [12]. Using the linear constitutive law for an orthotropic material, the in-plane stresses of a lamina are defined as

$$\boldsymbol{\sigma}_p = \mathbf{C}_p \boldsymbol{\varepsilon}_p^0 + z\,\mathbf{C}_p \boldsymbol{\kappa} \tag{16}$$

The force and moment resultants of a fiber-reinforced composite consisting of *N* orthotropic laminae can then be defined as

$$\mathbf{N} = \sum_{k=1}^{N} \mathbf{C}_p^k \int_{z_{k-1}}^{z_k} \boldsymbol{\varepsilon}_p^0 \, dz + \sum_{k=1}^{N} \mathbf{C}_p^k \int_{z_{k-1}}^{z_k} z\,\boldsymbol{\kappa} \, dz \tag{17}$$

and

$$\mathbf{M} = \sum_{k=1}^{N} \mathbf{C}_p^k \left(\int_{z_{k-1}}^{z_k} z\,\boldsymbol{\varepsilon}_p^0 \, dz \right) + \sum_{k=1}^{N} \mathbf{C}_p^k \left(\int_{z_{k-1}}^{z_k} z^2\,\boldsymbol{\kappa} \, dz \right) \tag{18}$$

where $\mathbf{N} = [N_x \quad N_y \quad N_{xy}]^T$, $\mathbf{M} = [M_x \quad M_y \quad M_{xy}]^T$, $\mathbf{C}_p^k$ is the material moduli matrix for the *k*-th layer, and z_k is the thickness coordinate at the upper surface of the *k*-th layer. It is important to notice here that the force and moment resultants are defined as forces and moments per unit length [12]. Since the strain and curvature are not function of the thickness coordinate *z* in the Kirchhoff plate theory, Eqs. 17 and 18 are written in a matrix form as [12]

$$\begin{bmatrix} \mathbf{N} \\ \mathbf{M} \end{bmatrix} = \begin{bmatrix} \mathbf{A} & \mathbf{B} \\ \mathbf{B} & \mathbf{D} \end{bmatrix} \begin{bmatrix} \boldsymbol{\varepsilon}_p^0 \\ \boldsymbol{\kappa} \end{bmatrix} \tag{19}$$

where $A_{ij} = \sum_{k=1}^{N} (C_p^k)_{ij} (z_k - z_{k-1})$, $B_{ij} = \sum_{k=1}^{N} (C_p^k)_{ij} (z_k^2 - z_{k-1}^2)/2$, and $D_{ij} = \sum_{k=1}^{N} (C_p^k)_{ij} (z_k^3 - z_{k-1}^3)/3$.

The presence of the matrix **B** implies the extension and bending/twisting coupling of a laminate. However, if each lamina above the mid-plane is identical to that below the mid-plane in both geometry and material properties (i.e., the laminate is mid-plane symmetric), the matrix **B** becomes identically zero (i.e., $B_{ij} = 0$) and the extension and bending/twisting coupling vanishes.

It is important to notice here that the extension and shear coupling still exists. Another important case is a balanced laminate, in which a laminate consists of a pair of laminae that have opposite fiber angles ($+\theta$ and $-\theta$) above and below the mid-plane, regardless of the stacking sequence. This eliminates the extension and shear coupling. That is, coupling terms of in-plane normal and in-plane shear strains in matrix **A** are identically zero. That is, for a two-layer laminate with the same layer thickness and opposite fiber angle ($+/-\theta$) about the mid-plane, the extension and shear coupling vanishes, but the extension and twisting coupling in **B** matrix exists. This causes twisting deformation of a laminated plate subjected to a uniaxial tensile loading [12]. The presence of such a complex coupling is discussed using the ANCF laminated shell element in the last part of this Section.

3.2 Generalization to Shear Deformable ANCF Laminated Shear Element

As discussed in Section 2, the continuum mechanics based ANCF shell element is formulated as a continuum solid that accounts for the three-dimensional stress state, thus the complex deformation coupling exhibited in laminates can be automatically considered without special elastic force formulations. That is, the generalized elastic force of the laminated shell element that consists of *N* layers can be defined as follows:

$$\mathbf{Q}_s^i = -\sum_{k=1}^{N} \int_{V_0^{ik}} \left(\frac{\partial \boldsymbol{\varepsilon}^{ik}}{\partial \mathbf{e}^i} \right)^T \frac{\partial W^{ik}(\hat{\boldsymbol{\varepsilon}}^{ik})}{\partial \boldsymbol{\varepsilon}^{ik}} dV_0^{ik} \tag{20}$$

In the preceding equation, the integration interval for the *k*-th layer in the thickness direction is from z_{k-1} to z_k. In other words, the element generalized elastic forces are evaluated layer by layer and the resulting generalized elastic forces of each layer are simply added together to define the elastic force vector of the laminated shell. It is important to notice here that there is no restriction in material models considered in each lamia, despite the fact the orthotropic material

law is the most popular material model used for reinforced composite materials. Two Gaussian integration points are used along the thickness when the elastic forces of *each* layer are evaluated.

Orthotropic Saint-Venant-Kirchhoff Material Model For an orthotropic Saint-Venant-Kirchhoff material, the material moduli $C^{ijkl} = \partial^2 W / \partial \varepsilon_{ij} \partial \varepsilon_{kl}$ of an orthotropic lamina in the material frame is defined as [13]

$$C^{ijkl} = (\mathbf{b}^i \cdot \mathbf{a}_a)(\mathbf{b}^j \cdot \mathbf{a}_b)(\mathbf{b}^k \cdot \mathbf{a}_c)(\mathbf{b}^l \cdot \mathbf{a}_d)\bar{C}^{abcd} \tag{21}$$

where $(\mathbf{J}^i)^{-1} = [\mathbf{b}^1 \quad \mathbf{b}^2 \quad \mathbf{b}^3]$ and $\bar{C}^{abcd}$ is the tangent material moduli defined using 9 material parameters in the fiber coordinate system $[\mathbf{a}_1 \quad \mathbf{a}_2 \quad \mathbf{a}_3]$ as shown in Fig. 1, where the direction of fiber is defined along the coordinate 1. The material moduli $\bar{C}^{abcd}$ in the fiber coordinate system are given as follows [13]:

$$[\bar{C}^{ijkl}] = \begin{bmatrix} \bar{C}^{1111} & \bar{C}^{1122} & 0 & \bar{C}^{1133} & 0 & 0 \\ \bar{C}^{1122} & \bar{C}^{2222} & 0 & \bar{C}^{2233} & 0 & 0 \\ 0 & 0 & \bar{C}^{1212} & 0 & 0 & 0 \\ \bar{C}^{1133} & \bar{C}^{2233} & 0 & \bar{C}^{3333} & 0 & 0 \\ 0 & 0 & 0 & 0 & \bar{C}^{2323} & 0 \\ 0 & 0 & 0 & 0 & 0 & \bar{C}^{1313} \end{bmatrix} \tag{22}$$

where

$$\begin{aligned} &\bar{C}^{1111} = E_1(1-\nu_{23}\nu_{32})/\Delta \quad && \bar{C}^{2222} = E_2(1-\nu_{13}\nu_{31})/\Delta \quad && \bar{C}^{3333} = E_3(1-\nu_{12}\nu_{21})/\Delta \\ &\bar{C}^{1122} = E_1(\nu_{21}+\nu_{31}\nu_{23})/\Delta \quad && \bar{C}^{1133} = E_3(\nu_{13}+\nu_{12}\nu_{23})/\Delta \quad && \bar{C}^{2233} = E_2(\nu_{32}+\nu_{12}\nu_{31})/\Delta \\ &\bar{C}^{1212} = G_{12} && \bar{C}^{2323} = G_{23} && \bar{C}^{1313} = G_{13} \end{aligned} \tag{23}$$

and $\Delta = 1-\nu_{12}\nu_{21}-\nu_{23}\nu_{32}-\nu_{31}\nu_{13}-2\nu_{21}\nu_{32}\nu_{13}$.

Mooney-Rivlin Material Model For modeling incompressible materials such as rubbers, Mooney-Rivlin material model is widely used. The energy density function is defined as [14]

$$W = C_1(\bar{I}_1 - 3) + C_2(\bar{I}_2 - 3) + \frac{K}{2}(J-1)^2 \tag{24}$$

where C_1 and C_2 are material constants, $\bar{I}_1 = I_1/(I_3)^{1/3}$, $\bar{I}_2 = I_2/(I_3)^{2/3}$ and $J = (I_3)^{1/2}$, where I_1, I_2 and I_3 are invariants of right Cauchy-Green tensor [14]. K is a bulk modulus. The second Piola–Kirchhoff stress tensor **S** is obtained by differentiating the energy density function W with respect to Green-Lagrange strain tensor **E** as

$$\mathbf{S} = \frac{\partial W}{\partial \mathbf{E}} = 2C_1 (I_3)^{-1/3} \left(\mathbf{I} - \frac{1}{3} I_1 \mathbf{C}^{-1} \right) + 2C_2 (I_3)^{-2/3} \left(I_1 \mathbf{I} - \mathbf{C} - \frac{2}{3} I_2 \mathbf{C}^{-1} \right) + KJ(\mathrm{J}-1)\mathbf{C}^{-1} \qquad (25)$$

Equations of Motion Using the principle of virtual work in dynamics, the equations of motion of the shear deformable laminated shell element i can be expressed as

$$\mathbf{M}^i \ddot{\mathbf{e}}^i = \mathbf{Q}_s^i(\mathbf{e}^i, \boldsymbol{\alpha}^i) + \mathbf{Q}_e^i(\mathbf{e}^i, \dot{\mathbf{e}}^i, t) \qquad (26)$$

where vectors $\mathbf{Q}_s^i$ and $\mathbf{Q}_e^i$ are, respectively, the element elastic and external force vectors; and the matrix $\mathbf{M}^i$ is the constant element mass matrix defined by

$$\mathbf{M}^i = \sum_{k=1}^{N} \int_{V_0^{ik}} \rho_0^{ik} (\mathbf{S}^i)^T \mathbf{S}^i dV_0^{ik} \qquad (27)$$

where ρ_0^{ik} is the material density of k-th layer at the reference configuration. The internal parameters $\boldsymbol{\alpha}^i$ introduced for the enhanced assumed strains are determined by solving the following equations [10, 11]:

$$\int_{V_0^i} \left(\frac{\partial \boldsymbol{\varepsilon}^{EAS}}{\partial \boldsymbol{\alpha}^i} \right)^T \frac{\partial W^i(\hat{\boldsymbol{\varepsilon}}^i)}{\partial \boldsymbol{\varepsilon}^i} dV_0^i = \mathbf{0} \qquad (28)$$

It is important to notice here that the preceding equations can be solved at element level for the unknown internal parameters $\boldsymbol{\alpha}^i$ using the procedure presented in the literature [5].

3.3 Comparison with Analytical Solutions

To validate the ANCF laminated shell element presented in this Section, a uniaxial tensile test of

a two-layer laminate at $+/-\theta$ fiber angles is considered as a benchmark problem as shown in Fig. 2 [12]. The length, width and thickness of the laminated plate are 2.0 m, 1.0 m, and 0.01 m, respectively. The thicknesses of both layers are same (i.e., 0.005 m), but the sign of the fiber angles of the upper and lower layers are opposite as shown in Fig. 2. The tensile distributed uniaxial load of 500 N/m is applied in the *X* direction. As discussed in Section 3.1, the extension and bending/twisting coupling described by **B** matrix in Eq. 19 are not zero in this laminate, causing the warpage (twisting) under the uniaxial tensile loading [12]. It is also important to notice in this example that the extension and shear coupling exists in each lamina. However, shear deformation of the upper and lower layers developed by the uniaxial tensile load are same in magnitude, but opposite in direction. For this reason, the shear deformations of both layers are canceled out and no in-plane shearing occurs at the laminate level. That is, the extension and shear coupling term of **A** matrix of the laminate in Eq. 19 is identically zero in this problem. To demonstrate this fundamental coupling behavior of the laminated composite material using the ANCF laminated shell element, twisting angles of the two-layer laminated plate are presented in Fig. 3 as a function of the fiber angle θ. In this figure, results obtained by the ANCF laminated shell element, the laminated solid shell element in ANSYS (SOLSH190), and the analytical model discussed in Section 3.1 are compared. In the analytical model, the warpage is defined by [12]

$$w = -\frac{1}{2}\left(\kappa_x x^2 + \kappa_y y^2 + \kappa_{xy} xy\right) \tag{29}$$

and the curvature vector $\boldsymbol{\kappa} = [\kappa_x \quad \kappa_y \quad \kappa_{xy}]^T$ is determined by solving the following equation:

$$\begin{bmatrix} \boldsymbol{\varepsilon}_p^0 \\ \boldsymbol{\kappa} \end{bmatrix} = \begin{bmatrix} \mathbf{A} & \mathbf{B} \\ \mathbf{B} & \mathbf{D} \end{bmatrix}^{-1} \begin{bmatrix} \mathbf{N} \\ \mathbf{M} \end{bmatrix} \tag{30}$$

for $\mathbf{N} = [N_x \quad 0 \quad 0]^T$ and $\mathbf{M} = [0 \quad 0 \quad 0]^T$. It is observed from Fig. 3 that the twisting deformation obtained by the three different models agree well, and the warpage developed by the uniaxial tensile load applied to the two-layer laminated plate is well predicted by the ANCF laminated shell element developed in this study. It is important to notice here that the sign of the twisting angle of the composite plate changes at the fiber angle of $\theta = 54.7$ degree, and this important fiber angle is also correctly predicted with the ANCF laminated shell element.

4. APPLICATION TO PHYSICS-BASED ANCF TIRE MODEL

A tire has a complex structure that consists of layers of plies and steel belts that are embedded in rubber, thus an accurate modeling of the complex tire geometry and the anisotropic material properties is essential to the tire performance evaluation including the tire contact pressure and the braking/traction and cornering forces. While the in-plane tire belt deformation can be modeled by an equivalent material model [3,4], such a simplified material model cannot be used for predicting the overall tire structural deformation in the three-dimensional analysis. This is attributed to the fact that the tire section property in both geometry and material is of crucial importance in characterizing the contact pressure distribution. This necessitates various fiber-reinforced rubber material models that can be integrated into high-fidelity finite element tire models [15,16]. However, despite the fact that accurate solutions can be obtained using existing finite element tire models, difficulties arise when they are integrated into the vehicle dynamics simulation due to the essential difference in formulations and solution procedures used in multibody dynamics and nonlinear finite element codes. This prevents an integration of the high-fidelity tire model into the multibody vehicle dynamics simulation. That is, the structural characteristics of tires and transient tire forces are, in many cases, evaluated using different computational models and different simulation approaches. For this reason, a physics-based

absolute nodal coordinate formulation tire model using the shear deformable laminated shell elements is developed such that the high-fidelity ANCF tire model can be integrated into general multibody dynamics computer algorithms for ground mobility simulation.

To this end, the tire cross section geometry is imported from the tire cut section and data points are interpolated by a cubic smoothing spline for extracting the nodal position and slope coordinates. As shown in Fig. 4, the tire cross-section is divided into the tread, sidewall, and bead sections. The number of layers, cord angles of layers, material properties are provided in each section to create the tire model data as shown in Fig. 5. The tread section consists of a carcass ply, two steel belts, a belt cover, and tread blocks. The carcass ply and steel belt are modeled as an orthotropic material with nylon and steel cords embedded in rubber, respectively. A rubber layer is considered between the upper and lower steel belts and between the carcass ply and the lower steel belt. The sidewall section is modeled by two carcass plies and a rubber that lies in between. The bead section is modeled by two carcass plies, a steel belt, and a rubber as shown in Fig. 5. Having determined the cross-section property, the three-dimensional tire geometry is generated by rotating the tire section model and the nodal coordinates of the ANCF tire model are created as summarized in Fig. 4.

The tire air pressure is 220 kPa that is considered by the normal distributed load applied to the inner surface of the tire. The penalty approach is used for modeling the normal contact force at each node in contact. The load-deflection curve is important for characterizing the fundamental structural properties of tires. The lateral and vertical deflections of the ANCF tire model shown in Fig. 6 are compared with the measurement results in Figs. 7 and 8. It is observed from these figures that the local tire deflections are well predicated in both lateral and vertical directions for the various wheel loads. Furthermore, the lengths of the contact patch in the longitudinal and

lateral directions also agree well with those of the measurement results as shown in Fig. 9 and 10.

5. SUMMARY AND CONCLUSIONS

In this study, a continuum mechanics based shear deformable shell element of the absolute nodal coordinate formulation (ANCF) is generalized to a laminated shell element for application to the modeling of fiber-reinforced rubber (FRR) structure of the physics-based ANCF tire model. It is shown that the complex deformation coupling exhibited in fiber-reinforced composite materials can be automatically considered in the shear deformable laminated shell element using the continuum mechanics approach. Furthermore, the element lockings are systematically eliminated by the assumed natural strain and enhanced strain approaches, thereby leading to a locking-free shear deformation ANCF laminated shell element. The benchmark problem of the extension and twisting coupling of two-layer laminated plate is used to validate the ANCF laminated shell element. The numerical results are in good agreement with those predicated by the analytical model based on the classical lamination theory and the laminated solid shell element in ANSYS. Furthermore, using the ANCF laminated shell element developed, a physics-based ANCF tire model is developed by considering the detailed tire geometry and material properties. The fiber-reinforced rubber is considered for modeling the carcass plies and steel belts using the multi-layered laminated shell elements. The load-deflection curves predicted by the physics-based ANCF tire model are in good agreement with the measurement results. In the future work, the tangential tire force model based on the distributed LuGre friction model is integrated into the ANCF tire model (ANCF-LuGre tire model) for use in the transient braking/traction and cornering force evaluation of tires in the context of multibody vehicle dynamics simulation.

ACKNOWLEDGEMENTS

This research is supported by the Automotive Research Center (ARC) in accordance with Cooperative Agreement W56HZV-04-2-0001 U.S. Army Tank Automotive Research, Development and Engineering Center (TARDEC).

REFERENCES

[1] Clark, S. K. (ed.), 1981, *Mechanics of Pneumatic Tires*, US DOT HS805 952 NHTSA.

[2] Sugiyama, H., Yamashita, H. and Jayakumar, P., 2014, "Right on Tracks - An Integrated Tire Model for Ground Vehicle Simulation from the University of Iowa", *Tire Technology International*, vol. 67, pp. 52-55.

[3] Sugiyama, H. and Suda, Y., 2009, "Nonlinear Elastic Ring Tire Model Using the Absolute Nodal Coordinate Formulation", *IMechE Journal of Multi-Body Dynamics*, vol. 223, pp. 211-219.

[4] Yamashita, H., Matsutani, Y. and Sugiyama, H., "Longitudinal Tire Dynamics Model for Transient Braking Analysis: ANCF-LuGre Tire Model", *ASME Journal of Computational and Nonlinear Dynamics*, in press.

[5] Yamashita, H., Valkeapää, A., Jayakumar, P. and Sugiyama, H., "Continuum Mechanics Based Bi-Linear Shear Deformable Shell Element using Absolute Nodal Coordinate Formulation", *ASME Journal of Computational and Nonlinear Dynamics*, in press.

[6] Shabana, A. A., *Dynamics of Multibody Systems*, 2005, Cambridge University Press, New York.

[7] Gerstmayr, J., Sugiyama, H., and Mikkola, A., 2013, "Review on the Absolute Nodal Coordinate Formulation for Large Deformation Analysis of Multibody Systems", *ASME Journal of Computational and Nonlinear Dynamics*, vol. 8, pp. 031016-1-12.

[8] Dvorkin, E. N., and Bathe, K. J., 1984, "A Continuum Mechanics Based Four-Node Shell Element for General Non-Linear Analysis", *Engineering Computations*, vol. 1, pp.77-88.

[9] Betsch, P., and Stein, E., 1995, "An Assumed Strain Approach Avoiding Artificial Thickness Straining for A Non-Linear 4-Node Shell Element", *Communications in Numerical Methods in Engineering*, vol. 11, pp. 899-909.

[10] Simo, J. C., and Rifai, M. S., 1990, "A Class of Mixed Assumed Strain Methods and The Method of Incompatible Modes", *International Journal for Numerical Methods in Engineering*, vol. 29, pp.1595-1638.

[11] Andelfinger, U., and Ramm, E., 1993, "EAS-Elements for Two-Dimensional, Three-Dimensional, Plate and Shell Structures and Their Equivalence to HR-Elements", *International Journal for Numerical Methods in Engineering*, vol. 36, pp.1311-1337.

[12] Jones, R. M., 1999, *Mechanics of Composite Materials*, Taylor and Francis.

[13] Vu-Quoc, L., and Tan, X. G., 2003, "Optimal Solid Shells for Non-Linear Analyses of Multilayer Composites: I Statics", *Computer Methods in Applied Mechanics and Engineering*, vol. 192, pp. 975-1016.

[14] Bathe, K.J., *Finite Element Procedures*, 1996, Prentice Hall.

[15] Lee, C.R., Kim, J.W., Hallquist, J.O., Zhang, Y. and Farahani, A.D., 1997, "Validation of a FEA Tire Model for Vehicle Dynamic Analysis and Full Vehicle Real Time Proving Ground Simulations", *SAE Technical Paper 971100*.

[16] Gruber, P., Sharp, R. S. and Crocombe, A. D., 2012, "Normal and Shear Forces in the Contact Patch of a Braked Racing Tyre. Part 2: Development of a Physical Tyre Model", *Vehicle System Dynamics*, vol. 50, pp. 339-356.

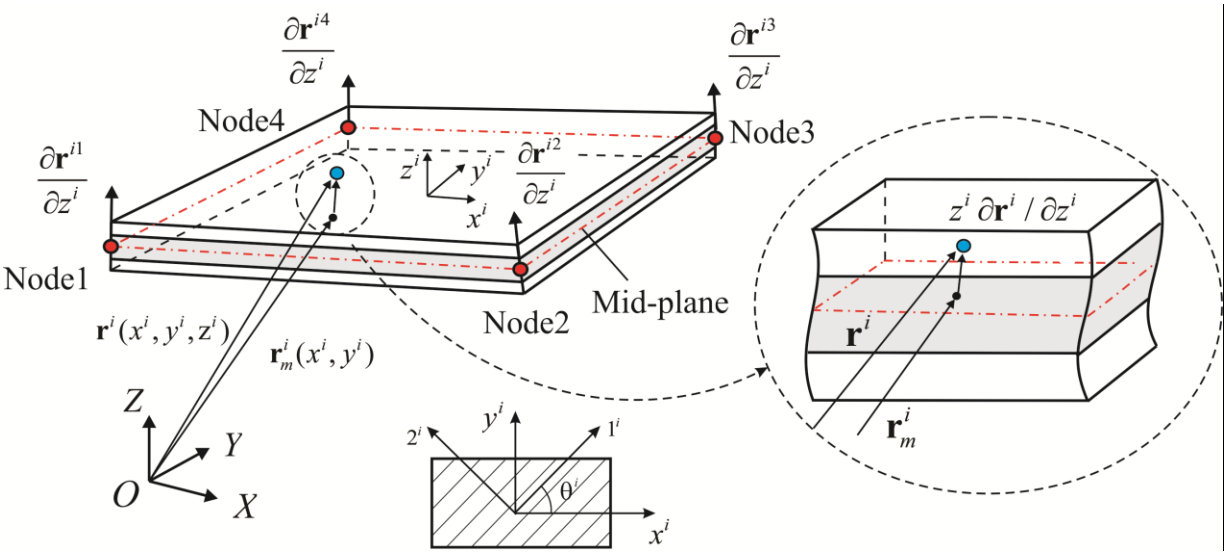

Figure 1. Kinematics of shear deformable ANCF laminated shell element

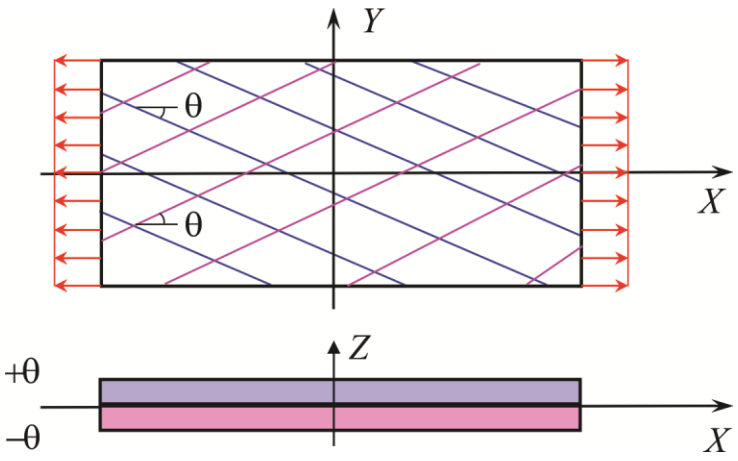

Figure 2. Uniaxial tensile test of two-layer laminate

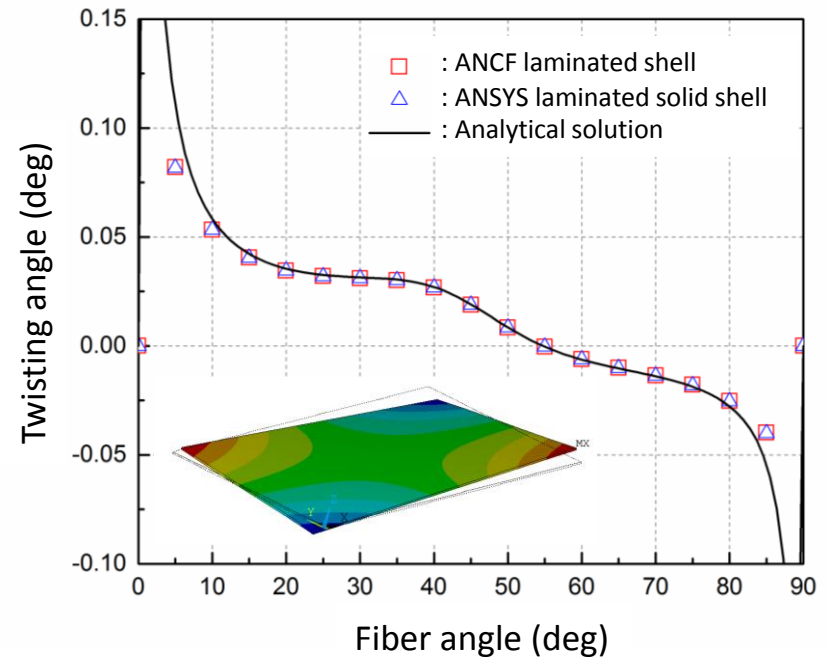

Figure 3. Twisting of two-layer laminate subjected to uniaxial tensile load

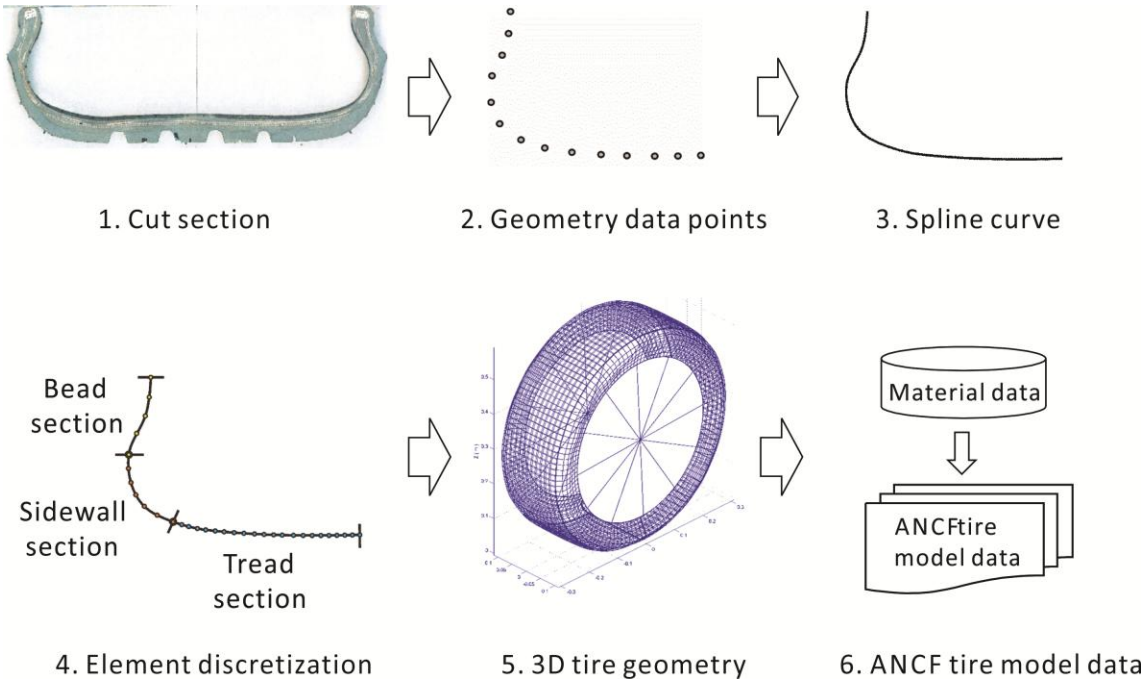

Figure 4. ANCF tire model creation procedure

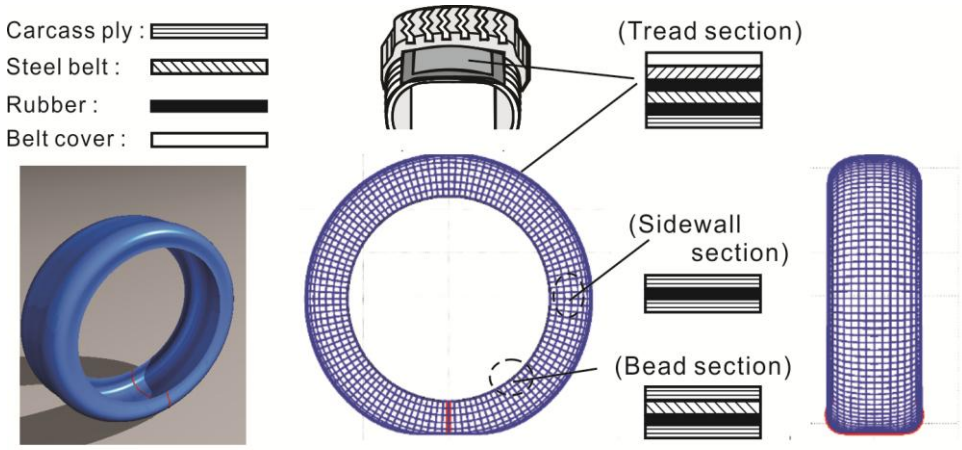

Figure 5. Physics-based ANCF tire model using multi-layered laminated shell element

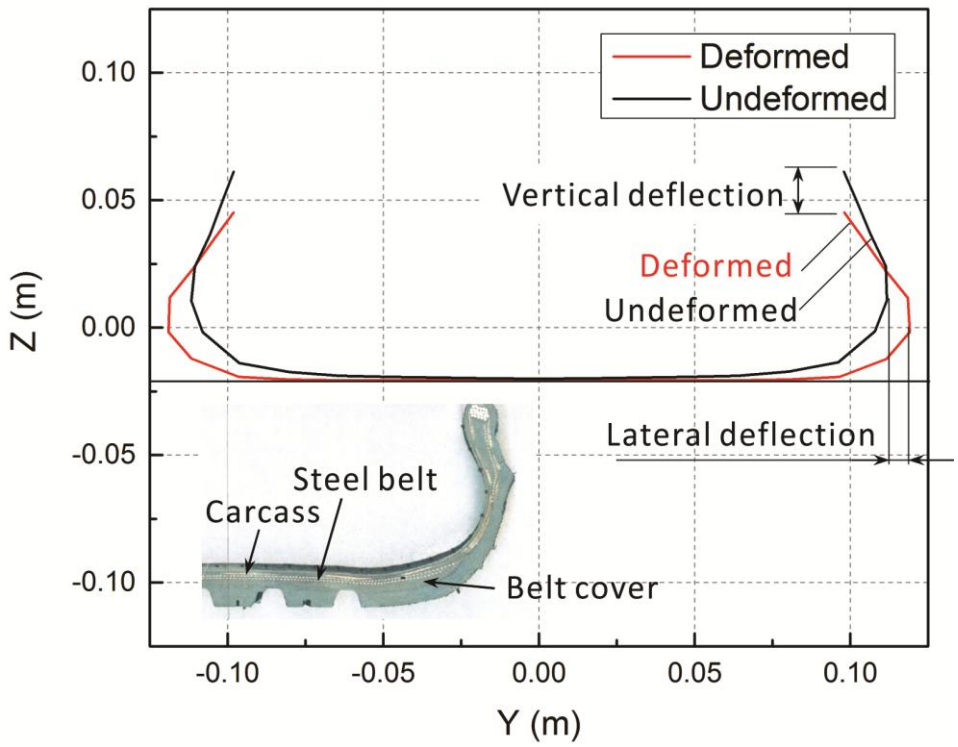

Figure 6. Deformed shape of tire cross section

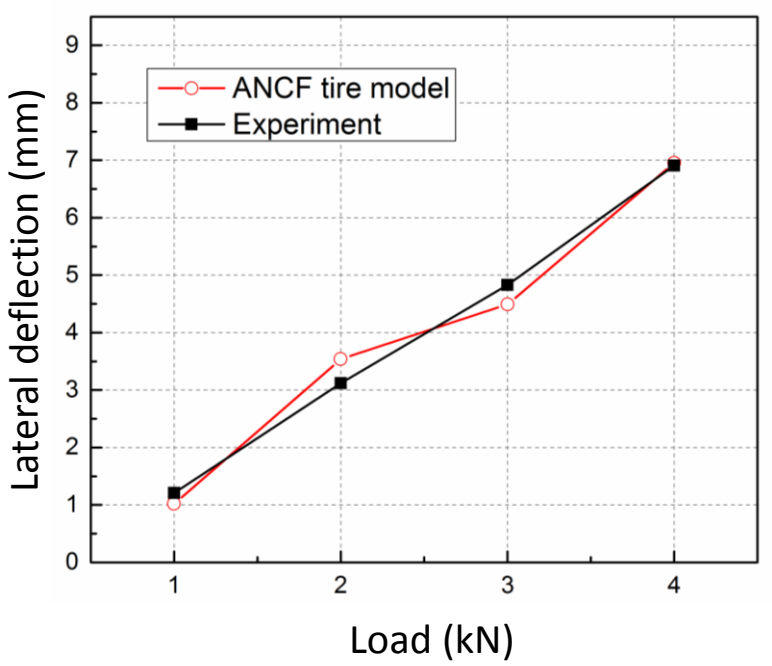

Figure 7. Lateral deflection of tire for various wheel loads

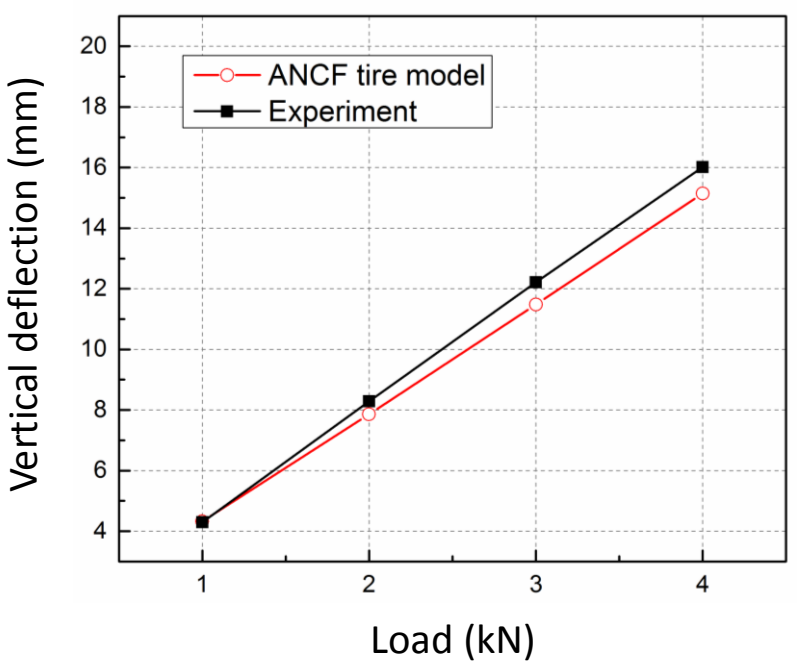

Figure 8. Vertical deflection of tire for various wheel loads

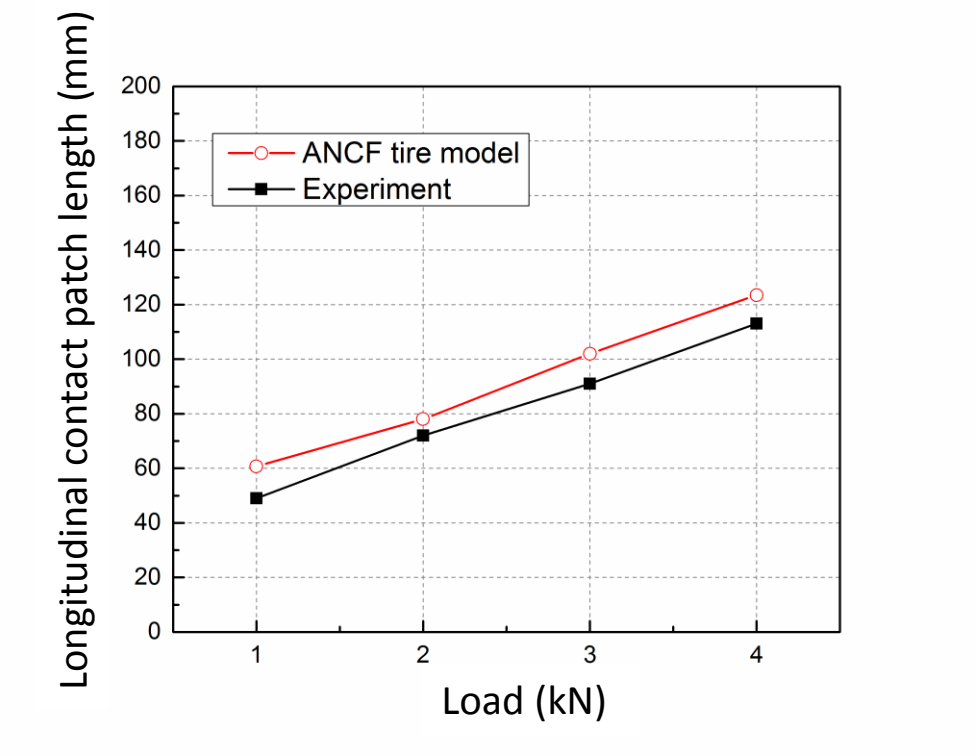

Figure 9. Longitudinal contact patch length for various wheel loads

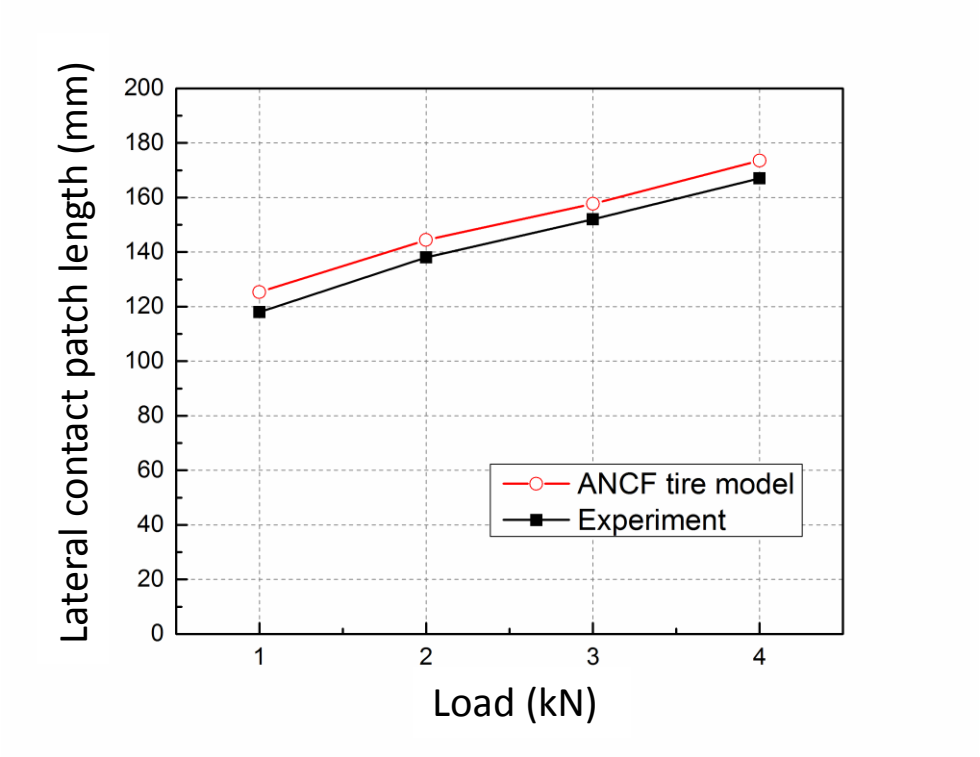

Figure 10. Lateral contact patch length for various wheel loads